Kinetics, selectivity and scale up of the Fischer-Tropsch synthesis

van der Laan, Gerard Pieter

5

Intrinsic Kinetics of the Gas-Solid Fischer-Tropsch and Water Gas Shift Reactions

Abstract

The kinetics of the gas-solid Fischer-Tropsch synthesis over a commercial Fe-Cu-K-SiO_2 catalyst was studied in a continuous spinning basket reactor. Experimental conditions were varied as follows: reactor pressure of 0.8-4.0 MPa, H_2/CO feed ratio of 0.25-4.0, and space velocity of 0.5-2.0 10^{-3} Nm^3 kg_{cat}^{-1} s^{-1} at a constant temperature of 523 K. A number of rate equations were derived on the basis of a detailed set of possible reaction mechanisms originating from the carbide mechanism for the hydrocarbon formation and the formate mechanism for the water gas shift reaction, respectively. 14 models for the Fischer-Tropsch reaction rate and 2 water gas shift reaction rate models were fitted to the experimental reaction rates. Bartlett's test was used to reduce the set of Fischer-Tropsch rate equations to 3 models, which were statistically indistinguishable. It could be concluded that the reaction rate of the Fischer-Tropsch synthesis is controlled by the formation of the monomer species (methylene) by hydrogenation of molecularly adsorbed CO, whereas the carbon dioxide formation rate (water gas shift) is determined by the formation of a formate intermediate species from adsorbed CO and dissociated hydrogen. Simulations using the optimal kinetic models derived showed good agreement both with experimental data and with some kinetic models from literature.

5.1 Introduction

The Fischer-Tropsch synthesis can be simplified as a combination of the FT reaction and the water gas shift (WGS) reaction. Water is a primary product of the FT reaction, and CO_2 can only be produced by the WGS reaction ($R_{WGS} = R_{CO_2}$). The water gas shift reaction is a reversible parallel-consecutive reaction with respect to CO (see Figure 5.1).

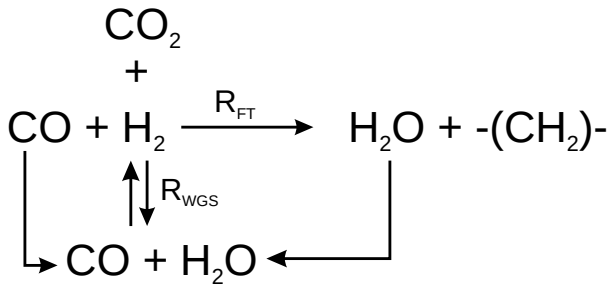

Figure 5.1 Scheme of the reaction of carbon monoxide and hydrogen.

The major problem in describing Fischer-Tropsch reaction kinetics is the complexity of its reaction mechanism and the large number of species involved. Literature on the kinetics of the Fischer-Tropsch synthesis can be divided into two classes. Most studies aim at catalyst improvement and postulate empirical power law kinetics for the carbon monoxide rates [1, 2]:

$$-R_{CO} = k\ P_{H_2}^{a}\ P_{CO}^{b} \tag{5.1}$$

and carbon dioxide formation or water gas shift reaction [3, 4]:

$$R_{CO_2} = k\ P_{H_2O}^{c}\ P_{CO}^{d} \tag{5.2}$$

Relatively few studies aim at understanding the reaction mechanisms. Some authors derived Langmuir-Hinshelwood- Hougen-Watson (LHHW) rate expressions for the reactant consumption [5, 6]. In most cases the rate determining step was assumed to be the formation of the building block or monomer, methylene [7–14]. Simultaneous modeling of the WGS and FT reactions on iron catalysts with WGS activity has hardly been reported. Zimmerman and Bukur [9] and Shen et al. [15] fitted kinetic expressions to their data, but their rate expressions for the WGS were largely empirical.

Our objective is to develop intrinsic rate expressions for the CO conversion to Fischer-Tropsch products and for the water gas shift (WGS) reaction over a precip-

itated iron catalyst on the basis of realistic mechanisms. It also appeared that several existing literature models can be derived from the same limited set of mechanisms [7–14]. A reactor model will be used to predict the reaction rates and conversions as a function of experimental conditions. Comparison between the new rate expressions and available literature models is included as well. The kinetics of the gas-solid Fischer-Tropsch synthesis over a commercial Fe-Cu-K-SiO_2 catalyst were studied in a continuous spinning basket reactor (CSTR) at industrially relevant conditions. Product distributions at the same reaction conditions are reported in Chapter 4.

5.2 Theory

5.2.1 Active Sites on Precipitated Iron Catalysts

The composition of iron-based catalysts changes during Fischer-Tropsch synthesis. Zhang and Schrader [16] concluded that two active sites operate simultaneously on the surface of iron catalysts: Fe^0/Fe-carbides and magnetite (Fe_3O_4). The carbide phase is active towards dissociation of CO and formation of hydrocarbons, while the oxide phase adsorbs CO associatively and produces predominantly oxygenated products. Lox et al. [17] and Shroff et al. [18] concluded that the magnetite phase has negligible catalytic activity towards FT reactions whereas carbide formation results in a high FT activity.

Several authors proposed that magnetite (Fe_3O_4) is the most active phase for the WGS reaction [4, 5, 16, 19, 20] on iron catalysts. Rao et al. [19] studied the iron phase of Fe/Cu/K/SiO_2 catalysts from the demonstration unit at LaPorte, Texas (August, 1992) with Mössbauer spectroscopy. The changes of the magnetite phase corresponded with the WGS reaction activity during time-on-stream. Lox et al. [17] showed that Fe_3O_4 coexists with various iron carbides on the catalyst during synthesis gas reactions. It is generally accepted that the WGS and FT reactions proceed on different active sites on precipitated iron catalysts [5, 19].

5.2.2 Hydrocarbon Formation

5.2.2.1 Elementary Reactions

The mechanism of the hydrocarbon formation during the FTS has been reviewed and discussed by several authors [1, 21–24]. Recent reviews were given by Hindermann et al. [25], Dry [26], Dry [27], and Adesina [28] and in Chapter 2. The most important

growth mechanism for the hydrocarbon formation is the surface carbide mechanism by CH_2 insertion [1, 6, 29, 30]. The presence of adsorbed methylene has been identified with isotopic-tracer techniques on Fe/Al_2O_3 [31].

The formation of the methylene species will be discussed in more detail. Hydrogen reacts via either the dissociative adsorbed state or in the molecular state [32]. Dissociative adsorption of hydrogen proceeds on two free active sites:

$$H_2 + 2s_1 \rightleftarrows 2Hs_1 \tag{5.3}$$

s_1 denotes a catalytic site where hydrocarbons can be formed. Carbon monoxide adsorbs associatively on an active site [32]:

$$CO + s_1 \rightleftarrows COs_1 \tag{5.4}$$

Adsorbed CO can be dissociated in a second step:

$$COs_1 + s_1 \rightleftarrows Cs_1 + Os_1 \tag{5.5}$$

Surface carbon reacts with adsorbed dissociated hydrogen,

$$Cs_1 + Hs_1 \rightleftarrows CHs_1 + s_1 \tag{5.6}$$

$$CHs_1 + Hs_1 \rightleftarrows CH_2s_1 + s_1 \tag{5.7}$$

or with molecular hydrogen,

$$Cs_1 + H_2 \rightleftarrows CH_2s_1 \tag{5.8}$$

Oxygen is removed irreversibly and rapidly from the surface by consecutive hydrogenation reactions [24, 33, 34],

$$Os_1 + Hs_1 \rightarrow HOs_1 + s_1 \tag{5.9}$$

$$HOs_1 + Hs_1 \rightarrow H_2Os_1 + s_1 \tag{5.10}$$

$$H_2Os_1 \rightleftarrows H_2O + s_1 \tag{5.11}$$

or with molecular hydrogen according to an Eley-Rideal mechanism [8, 24, 33],

$$Os_1 + H_2 \rightarrow H_2Os_1 \tag{5.12}$$

$$H_2Os_1 \rightleftarrows H_2O + s_1 \tag{5.13}$$

Another possible mechanism starts with molecularly adsorbed carbon monoxide and successive hydrogen assisted dissociation with dissociated hydrogen [6, 8],

$$COs_1 + Hs_1 \rightleftarrows HCOs_1 + s_1 \tag{5.14}$$

$$HCOs_1 + Hs_1 \rightleftarrows Cs_1 + H_2Os_1 \tag{5.15}$$

or molecular hydrogen,

$$COs_1 + H_2 \rightleftarrows HCOHs_1 + s_1 \tag{5.16}$$

$$HCOHs_1 + H_2 \rightleftarrows CH_2s_1 + H_2O \tag{5.17}$$

Based on these elementary reactions, we defined four different possible mechanisms. See Table 5.1 for the conventions and state of the reactants in the elementary formation reactions of methylene. The complete set of elementary reactions for each model is given in Table 5.2.

Table 5.1 The various kinetic models considered, together with the presence of the reactants in the rate determining step.

Model	CO	H_2
FT-I	Dissociative	Dissociative
FT-II	Dissociative	Molecular
FT-III	Associative	Dissociative
FT-IV	Associative	Molecular

5.2.2.2 Kinetic Rate Equations

In order to derive rate equations, we used the Langmuir-Hinshelwood-Hougen-Watson approach, see, for example, Graaf et al. [35]. For each model, the possible rate determining steps were identified, while all other steps were assumed to be at quasi-equilibrium. The following assumptions, all based on literature, were taken into account:

1. Reaction path for the CO consumption to the monomer methylene, CH_2, contains one irreversible rate determining step, in analogy with Ref. [35].

2. Steady state concentrations of all intermediates on the catalyst surface [35, 36].

Table 5.2 Elementary reactions for FT synthesis.

Model	Number	Elementary reaction
FT-I	1	$CO + s_1 \rightleftarrows COs_1$
	2	$COs_1 + s_1 \rightleftarrows Cs_1 + Os_1$
	3	$Cs_1 + Hs_1 \rightleftarrows CHs_1 + s_1$
	4	$CHs_1 + Hs_1 \rightleftarrows CH_2s_1 + s_1$
	5	$Os_1 + Hs_1 \rightarrow HOs_1 + s_1$
	6	$HOs_1 + Hs_1 \rightarrow H_2Os_1 + s_1$
	7	$H_2O + s_1 \rightleftarrows H_2Os_1$
	8	$H_2 + 2s_1 \rightleftarrows 2Hs_1$
FT-II	1	$CO + s_1 \rightleftarrows COs_1$
	2	$COs_1 + s_1 \rightleftarrows Cs_1 + Os_1$
	3	$Cs_1 + H_2 \rightleftarrows CH_2s_1$
	4	$Os_1 + H_2 \rightarrow H_2Os_1$
	5	$H_2O + s_1 \rightleftarrows H_2Os_1$
FT-III	1	$CO + s_1 \rightleftarrows COs_1$
	2	$COs_1 + Hs_1 \rightleftarrows HCOs_1 + s_1$
	3	$HCOs_1 + Hs_1 \rightleftarrows Cs_1 + H_2Os_1$
	4	$Cs_1 + Hs_1 \rightleftarrows CHs_1 + s_1$
	5	$CHs_1 + Hs_1 \rightleftarrows CH_2s_1 + s_1$
	6	$H_2 + 2s_1 \rightleftarrows 2Hs_1$
	7	$H_2O + s_1 \rightleftarrows H_2Os_1$
FT-IV	1	$CO + s_1 \rightleftarrows COs_1$
	2	$COs_1 + H_2 \rightleftarrows H_2COs_1$
	3	$H_2COs_1 + H_2 \rightleftarrows CH_2s_1 + H_2O$
	4	$H_2O + s_1 \rightleftarrows H_2Os_1$

[1]Equilibrium constant, e.g. reaction step FT-I1: $K_1 = \dfrac{\theta_{COs_1}}{P_{CO}\theta_{s_1}}$

Table 5.3 Reaction rate expressions considered for the Fischer-Tropsch synthesis, R_{FT} (mol kg_{cat}^{-1} s^{-1}).

Model	Kinetic equation
FT-I3	$\frac{k P_{CO}^{1/2} P_{H_2}^{1/2}}{\left(1 + a P_{CO}^{1/2} + b P_{H_2O}\right)^2}$
FT-I4	$\frac{k P_{CO}^{1/2} P_{H_2}^{3/4}}{\left(1 + a P_{CO}^{1/2} P_{H_2}^{-1/4} + b P_{H_2O}\right)^2}$
FT-II3	$\frac{k P_{CO}^{1/2} P_{H_2}}{1 + a P_{CO}^{1/2} + b P_{H_2O}}$
FT-III2	$\frac{k P_{CO} P_{H_2}^{1/2}}{\left(1 + a P_{CO} + b P_{H_2O}\right)^2}$
FT-III3	$\frac{k P_{CO} P_{H_2}}{\left(1 + a P_{CO} + b P_{H_2O}\right)^2}$
FT-IV2	$\frac{k P_{CO} P_{H_2}}{1 + a P_{CO} + b P_{H_2O}}$
FT-IV3	$\frac{k P_{CO} P_{H_2}^2}{1 + a P_{CO} + b P_{H_2O}}$

3. Catalyst sites of type 1 are active towards hydrocarbon formation, which are uniform and homogeneously distributed [35, 36].

4. Initial adsorption of hydrogen and carbon monoxide is in quasi-equilibrium with the gas phase concentrations [24].

5. Water is removed irreversibly after CO dissociation [24, 33, 37].

6. CO is adsorbed more strongly than H_2 on iron catalysts, resulting in a high surface concentration of CO or dissociated CO relative to H_2 [21, 38].

7. H_2O adsorbs strongly and may inhibit the FT reaction rate [9].

With these assumptions, 7 different kinetic models remain possible. These are summarized in Table 5.3. The development of the kinetic equations will be illustrated for model FT-II3. The model codes refer to the set of elementary reactions and the elementary reaction not at equilibrium (that is the rate determining step, so in this case

Table 5.4 Parameters for the FT kinetic models.

Model	k (x) (mol kg^{-1} s^{-1} MPa^x)	a (x) (MPa^x)	b (MPa^{-1})
FT-I3	$(k_3k_5K_1K_2K_8)^{1/2}$ (-1)	$(K_1K_2k_5/k_3)^{1/2}$ (-1/2)	K_7
FT-I4	$(k_4k_5K_1K_2K_3)^{1/2}K_8^{3/4}$ (-5/4)	$(K_1K_2K_3K_8^{1/2}k_5/k_4)^{1/2}$ (-1/4)	K_7
FT-II3	$(k_3k_4K_1K_2)^{1/2}$ (-3/2)	$(k_4K_1K_2/k_3)^{1/2}$ (-1/2)	K_5
FT-III2	$k_2K_1K_6^{1/2}$ (-3/2)	K_1 (-1)	K_7
FT-III3	$k_3K_1K_2K_6$ (-2)	K_1 (-1)	K_7
FT-IV2	k_2K_1 (-2)	K_1 (-1)	K_4
FT-IV3	$k_3K_1K_2$ (-3)	K_1 (-1)	K_4

reaction 3). The set of elementary reactions for model FT-II3 is shown in Table 5.2. The reaction rate of the rate determining step is:

$$R_{\text{FT-II3}} = k_3\theta_{Cs_1}P_{H_2} = k_4\theta_{Os_1}P_{H_2} \quad (\text{mol kg}_{cat}^{-1}\ \text{s}^{-1}) \tag{5.18}$$

The surface fraction of carbon can be calculated from the site balance, the preceding reaction steps which are at quasi-equilibrium and the reaction rate for water formation:

$$K_1 = \frac{\theta_{CO_{s_1}}}{P_{CO}\theta_{s_1}}, \quad K_2 = \frac{\theta_{C_{s_1}}\theta_{O_{s_1}}}{\theta_{CO_{s_1}}\theta_{s_1}} \tag{5.19}$$

$$\theta_{Cs_1} = \frac{k_4}{k_3}\theta_{Os_1} = \left(\frac{K_1K_2k_4}{k_3}\right)^{1/2} P_{CO}^{1/2}\theta_{s_1} \tag{5.20}$$

From assumptions 6 and 7 it follows that only surface carbon and water occupy a significant fraction of the total number of sites, the site balance becomes:

$$\theta_{s_1} + \theta_{Cs_1} + \theta_{H_2Os_1} = 1 \tag{5.21}$$

Substitution of the surface fraction of carbon in eq 5.18:

$$R_{\text{FT-II3}} = \frac{(k_3k_4K_1K_2)^{1/2}P_{CO}^{1/2}P_{H_2}}{1 + (K_1K_2k_4/k_3)^{1/2}P_{CO}^{1/2} + K_5P_{H_2O}} = \frac{kP_{CO}^{1/2}P_{H_2}}{1 + aP_{CO}^{1/2} + bP_{H_2O}} \tag{5.22}$$

Table 5.3 summarizes the final form of the various rate expressions for the 7 possible kinetic models considered, whereas Table 5.4 shows the kinetic and adsorption parameters for the different kinetic models. It can be seen that the pressure dependency of CO and H_2 in the numerator ranges from 1/2 to 1, and 1/2 to 2, respectively. The denominator is quadratic in case of a dual site elementary reaction, in contrast to a single

site rate determining step. The denominator consists of the individual contributions of significantly abundant species on the catalyst surface.

The concentration of free sites θ_{s_1} is determined from a site balance. It is assumed that the total number of sites is constant:

$$\theta_{s_1} + \sum_{i=1}^{n} \theta_{is_1} = 1 \tag{5.23}$$

where θ_{s_1} is the fraction free sites and θ_{is_1} are the surface fractions occupied with adsorbed species such as carbon, carbon monoxide, hydrogen, alkyl chains, water, carbon dioxide, and so forth The addition of several inhibition terms in the denominator can not be justified statistically due to a high degree of covariance or correlation [39, 40]. The derived kinetic expressions have a maximum of two inhibition terms: one term for CO or a carbidic species (θ_{Cs_1}) and the other for H_2O inhibition.

5.2.2.3 Literature Models

Reviews of kinetic equations for iron-based catalysts were published by Huff and Satterfield [8], Zimmerman and Bukur [9], and Van der Laan and Beenackers [45], enclosed in slightly revised form as Chapter 2. Kinetic studies of the FTS on iron and cobalt catalysts are summarized in Table 5.5. The corresponding operating conditions are given in Chapter 2 (Table 2.7).

It can be shown that all these literature models can be derived from the set of mechanisms considered in this study and which are summarized in Table 5.2. Appropriate assumptions for the inhibitor effects in the site balance of the kinetic rate expressions in table 5.3 result in similar mathematical expressions. The mechanistic implications of the available FT kinetic models are summarized in Table 5.5.

5.2.3 Water Gas Shift Reaction

5.2.3.1 Reaction Mechanism

Several mechanisms for the water gas shift reaction were proposed in the literature. Single studies of the water gas shift reaction over supported metals suggest the appearance of formate species [4, 5, 20, 35]. The formate species can be formed by the reaction between either a hydroxy species or water and carbon monoxide either in the gas phase or in the adsorbed state. The hydroxy intermediate can be formed by the decomposition of water. The formate intermediate can be reduced to either adsorbed or gaseous carbon dioxide (see Table 5.6). Rethwisch and Dumesic [20] studied the water gas shift reaction on several supported and unsupported iron oxide and zinc

Table 5.5 Reaction rate equations overall synthesis gas consumption rate. See Table 2.7 for experimental conditions, reactor type and catalyst applied.

	Kinetic expression	References	Mechanistic implications
(a)	kP_{H_2}	[9, 22, 41]	FT-II3 (b=0, $aP_{CO} \gg 1$) FT-IV2 (b=0, $aP_{CO} \gg 1$)
(b)	$kP_{H_2}^{a}P_{CO}^{b}$	[3]	-
(c)	$\frac{kP_{H_2}P_{CO}}{P_{CO}+KP_{H_2O}}$	[7, 9, 10, 15, 22]	FT-IV2 (aP_{CO} and $bP_{H_2O} \gg 1$)
(d)	$\frac{kP_{H_2}^{2}P_{CO}}{P_{CO}P_{H_2}+KP_{H_2O}}$	[8, 15, 42, 43]	FT-II3 (water formation is reversible)
(e)	$\frac{kP_{H_2}^{2}P_{CO}}{1+aP_{CO}P_{H_2}^{2}}$	[22]	-
(f)	$\frac{kP_{H_2}P_{CO}}{P_{CO}+KP_{CO_2}}$	[9, 11, 12, 43]	FT-IV2 ($aP_{CO} \gg 1$ and CO_2 inhibition)
(g)	$\frac{kP_{H_2}P_{CO}}{P_{CO}+K_1P_{H_2O}+K_2P_{CO_2}}$	[9, 11, 12]	FT-IV2 ($aP_{CO} \gg 1$, CO_2 and H_2O inhibition)
(h)	$\frac{kP_{CO}^{1/2}P_{H_2}^{1/2}}{\left(1+K_1P_{CO}^{1/2}+K_2P_{H_2}^{1/2}\right)^{2}}$	[14]	FT-I3 (H_2 inhibition, $bP_{H_2O}=0$)
(i)	$\frac{kP_{CO}P_{H_2}^{1/2}}{\left(1+K_1P_{CO}+K_2P_{H_2}^{1/2}\right)^{2}}$	[6]	FT-III2 (H_2 inhibition, $bP_{H_2O}=0$)
(j)	$\frac{kP_{CO}P_{H_2}}{(1+KP_{CO})^{2}}$	[13, 40, 44]	FT-III3 ($bP_{H_2O}=0$)

Table 5.6 Elementary reactions for the water gas shift reaction.

Model	Number	Elementary reaction
WGS-I	1	$CO + s_2 \rightleftarrows COs_2$
	2	$CO_2 + s_2 \rightleftarrows CO_2s_2$
	3	$H_2O + s_2 \rightleftarrows H_2Os_2$
	4	$H_2 + 2s_2 \rightleftarrows 2Hs_2$
	5	$COs_2 + H_2Os_2 \rightleftarrows HCOOs_2 + Hs_2$
	6	$HCOOs_2 + s_2 \rightleftarrows Hs_2 + CO_2s_2$
WGS-II	1	$CO + s_2 \rightleftarrows COs_2$
	2	$CO_2 + s_2 \rightleftarrows CO_2s_2$
	3	$H_2O + s_2 \rightleftarrows H_2Os_2$
	4	$H_2Os_2 + s_2 \rightleftarrows OHs_2 + Hs_2$
	5	$H_2 + 2s_2 \rightleftarrows 2Hs_2$
	6	$COs_2 + OHs_2 \rightleftarrows HCOOs_2 + s_2$
	7	$HCOOs_2 + s_2 \rightleftarrows Hs_2 + CO_2s_2$

oxide catalysts. They suggested that the WGS reaction over unsupported magnetite proceeds via a direct oxidation mechanism, while all supported iron catalysts operate via a mechanism with formate species due to limited change of oxidation state of the iron cations.

5.2.3.2 Kinetic Expressions

Several assumptions were made in order to derive the LHHW rate expressions:

- Steady state for the adsorbed species.
- One rate determining step in the sequence of elementary reactions over the complete range of experimental conditions.
- Surface concentrations of intermediate species are negligible [35].
- Active sites for the WGS (type 2) are different than the sites for the hydrocarbon forming reactions (type 1) [5].

- Rate determining step is a dual-site elementary reaction between two adsorbed species [5].
- Adsorption of reactants and desorption of products are at equilibrium.

With the mentioned assumptions two rate determining steps are possible. First, the rate determining step is (WGS-II6):

$$COs_2 + OHs_2 \rightleftarrows HCOOs_2 + s_2 \tag{5.24}$$

The hydroxyl species is formed by dissociation of water:

$$H_2O + 2s_2 \rightleftarrows OHs_2 + Hs_2 \tag{5.25}$$

Second, the reaction between adsorbed water and carbon monoxide (WGS-I5) can be rate determining:

$$COs_2 + H_2Os_2 \rightleftarrows HCOOs_2 + Hs_2 \tag{5.26}$$

On basis of the formate mechanism and the mentioned assumptions, two kinetic rate equations were developed. The expressions are given in Table 5.7. The adsorption of H_2 and CO_2 are assumed to be negligible relative to CO and H_2O [5, 9, 38]. Thus, the mass balance of the catalytic sites, s_2, is:

$$\theta_{s_2} + \theta_{H_2Os_2} + \theta_{COs_2} = 1 \tag{5.27}$$

Derivation of other kinetic expressions based on adsorption of more components is possible from the above equations. Since the WGS reaction is an equilibrium reaction, the reverse reaction has to be taken into account. For the temperature dependency of the equilibrium constant of the WGS reaction, K_P, the following relation was used (Graaf et al. [46]):

$$\log K_P = \log\left(\frac{P_{CO_2}P_{H_2}}{P_{H_2O}P_{CO}}\right)_{eq} = \left(\frac{2073}{T} - 2.029\right) \tag{5.28}$$

Kinetic studies of the WGS reaction under FT conditions on iron-based catalysts are summarized in Chapter 2 (Table 2.8).

Table 5.7 Rate expressions considered for the water gas shift reaction, R_{CO_2} (mol kg_{cat}^{-1} s^{-1}).

Model	Kinetic equation	Site balance
WGS-I5	$\frac{k_w \left(P_{CO} P_{H_2O} - P_{CO_2} P_{H_2}/K_P\right)}{\left(1 + K_1 P_{CO} + K_3 P_{H_2O}\right)^2}$ $k_w = k_5 K_1 K_3$ (mol kg^{-1} s^{-1} MPa^{-2})	s_2, COs_2, H_2Os_2
WGS-II6	$\frac{k_w \left(P_{CO} P_{H_2O}/P_{H_2}^{1/2} - P_{CO_2} P_{H_2}^{1/2}/K_P\right)}{\left(1 + K_1 P_{CO} + K_3 P_{H_2O}\right)^2}$ $k_w = k_5 K_1 K_3 K_4 K_5^{-1/2}$ (mol kg^{-1} s^{-1} $MPa^{-1.5}$)	s_2, COs_2, H_2Os_2

5.3 Experimental

The kinetics of both the Fischer-Tropsch synthesis and the water gas shift reaction over a commercial precipitated iron catalyst (Ruhrchemie LP33/81) were unraveled by relevant experiments in a Spinning Basket Reactor (SBR). For a detailed description of the experimental set-up, the catalyst applied, the analytic and the experimental procedures, see Chapter 3.

The baskets were loaded with 2.34 g of catalyst, with particle diameters between 0.125 and 0.160 mm. The catalyst was pretreated with a hydrogen flow rate of 8.33 10^{-4} Nm^3 kg_{cat}^{-1} s^{-1} according to Bukur et al. [47]. The reactor temperature was linearly increased from 293 to 553 K by 0.017 K /s. The reactor temperature was kept at 553 K for 24 hrs at atmospheric pressure. After catalyst reduction, synthesis gas was fed to the reactor which at standard conditions operated at 523 K, 1.50 MPa, $(H_2/CO)_{feed}$=2 and a space velocity of 1.51 10^{-3} Nm^3 kg_{cat}^{-1} s^{-1}.

Checking the criteria of Weisz and Prater [48] for the reactants CO and H_2 showed that no intraparticle diffusion limitations occurred at relevant experimental conditions, even not at the highest conversion rates. Here, it was conservatively assumed that the catalyst pores were filled with long-chain hydrocarbon waxes.

24 kinetic experiments were carried out in the SBR with the Ruhrchemie precipitated iron catalyst. The experimental conditions were varied as follows: P= 0.8 - 4.0 MPa, H_2/CO feed ratio= 0.25 - 4.0, and $\Phi_{v,0}^{in}/W$= 0.5 10^{-3} - 2.0 10^{-3} Nm^3 kg_{cat}^{-1} s^{-1} at a temperature of 523 K. At regular intervals, the standard experiment was repeated to

determine possible deactivation effects of the catalyst. A summary of the experimental results and operating conditions is given in Appendix A.

5.4 Results and Discussion

After an initial period of 100 hrs, a steady state was more or less obtained. The catalyst activity, reaction rate to hydrocarbon products (R_{FT}) and the rate of the water gas shift (R_{WGS}) did not change much over 1200 hrs time on stream (see Chapter 3; Figure 3.10a). The reaction rates were not corrected for catalyst aging due to the small effect of time on stream on the catalyst activity.

The preliminary screening of the Fischer-Tropsch kinetic expressions was performed with a maximum of two adsorbed species in the site balance. Every kinetic model was optimized with two different mathematical forms of the site balance:

$$\theta_{s_1} + (\theta_{Cs_1} \text{ or } \theta_{COs_1}) + \theta_{H_2Os_1} = 1 \tag{5.29}$$

$$(\theta_{Cs_1} \text{ or } \theta_{COs_1}) + \theta_{H_2Os_1} = 1 \tag{5.30}$$

For models based on the carbide mechanism (FT-I, FT-II), the carbidic species is surface carbon θ_{Cs_1}, formed by dissociation of CO. Models FT-III and FT-IV are based on associative adsorbed CO species θ_{COs_1}. The 7 kinetic equations were optimized with a non-linear optimization routine using both eqs 5.29 and 5.30 for the site balance. Contributions of species in the site balance were eliminated if the fitted adsorption coefficients were not significantly different from zero or had a significantly negative value. Table 5.8 shows the results of the kinetic models with the relative variance and their ranking. Four models are able to describe the experimental FT reaction rates with a relative variance less than 35 % and a maximum of three optimized parameters.

Bartlett's test was applied to investigate whether the differences in accuracy of the various models were statistically significant [49, 50]. This test compares a critical calculated χ_c^2 value (for details, see Chapter 3 or Jonker et al. [49]) with a tabulated χ_t^2 value [51]. If χ_c^2 exceeds the tabulated value, the model with the largest deviation was rejected and χ_c^2 was recalculated. Models were subsequently rejected, until χ_c^2 was below the tabulated value. Table 5.9 compares χ_c^2 with the tabulated χ_t^2 value for $H-1$ degrees of freedom. The table shows that the best five models ($H=5$) passed the test and are statistically indistinguishable. The best five models are, in succeeding order: FT-IV2 (eq 5.29), FT-III2, FT-III3, FT-IV2 (eq 5.30), FT-II3. Model FT-II3 was rejected from list of best models, because the optimized parameters of this model were unrealistic and the model just passed the Bartlett's test due to the large relative

Table 5.8 FT kinetic model screening.

Model	Site balance (eq)	s_{rel} (%)	Rank	Remarks
FT-I3	5.30	63.7	6	
FT-I4	5.30	65.9	9	
FT-II3	5.30	45.2	5	
FT-III2	5.29	30.0	2	
FT-III2	5.30	64.4	8	
FT-III3	5.29	30.9	3	
FT-III3	5.30	63.8	7	
FT-IV2	5.29	29.6	1	
FT-IV2	5.30	32.4	4	
FT-IV3	5.29, 5.30	-	-	$a < 0$

FT-I3, FT-I4,FT-II3 with site balance 5.29 results in $a < 0$

variance. The site balances of models FT-IV2 (eq 5.29) and FT-IV2 (eq 5.30) vary slightly only. Consequently, the model with the highest relative variance was rejected, i.e. FT-IV2 (eq 5.30).

Four experiments were found to be outliers in the three remaining models (Runs: 5, 17, 20, 23). The remaining models were fitted again with the reduced data set of 20 experimental reaction rates. Table 5.10 gives the optimized values of the parameters in these three models: FT-III2, FT-III3, FT-IV2. The three remaining kinetic expressions (FT-III2, FT-III3, and FT-IV2) are all based on the combined enol/carbide mechanism. The mathematical form of the equations is very similar, indicating a difficult discrimination procedure. Figure 5.2 compares the experimental and calculated reaction rates of these three models.

Kinetic expression FT-IV2 is similar to several literature models [7, 9, 10, 22] for iron catalysts (see Table 5.5). In this model, the rate determining step is a single site reaction between undissociated adsorbed CO and gaseous H_2. However, the literature models were developed from experiments in slurry phase or packed bed reactors. The major difference between these literature models and optimized model FT-IV2 is a significant number of free sites in the latter model. In our experiments, the catalyst particles are located in spinning baskets with a small amount of high-boiling hydrocarbons present in the catalyst pores.

Kinetic expressions FT-III2 and FT-III3 are also able to describe our experiments accurately. These models are also developed from the combined enol/carbide mecha-

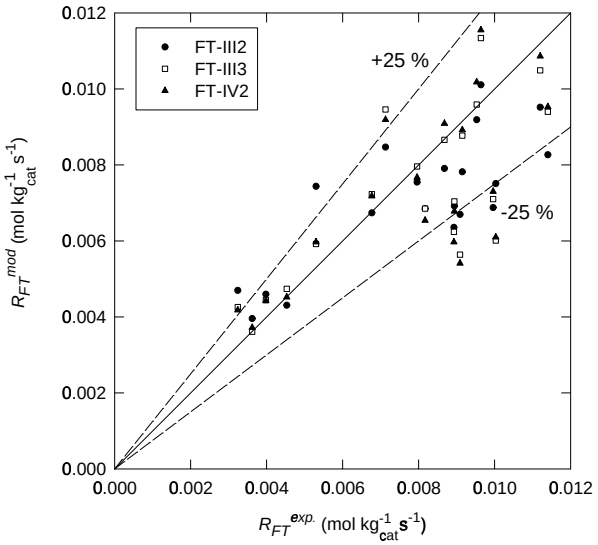

Figure 5.2 Parity graph of experimental and optimized Fischer-Tropsch reaction rates.

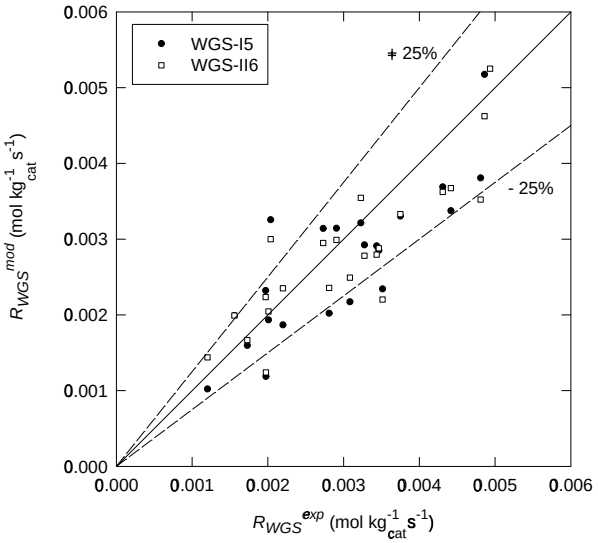

Figure 5.3 Parity graph of experimental and optimized WGS reaction rates.

Table 5.9 Bartlett's test for FT models[1].

H^2	χ_c^2	χ_t^2
9	42.2	15.5
8	38.2	14.1
7	32.6	12.6
6	23.6	11.1
5	6.03	9.49
4	0.206	7.81
3	0.040	5.99
2	0.0037	3.84

[1] χ_c^2: critical χ^2 according to Bartlett's test [49]; χ_t^2: tabulated χ^2 [51]

[2] H: number of models under consideration

nism: rate determining steps are the dual site surface reaction between undissociated adsorbed CO and dissociated H_2 (FT-III2) and between adsorbed formyl and dissociated H_2 (FT-III3). Model FT-III2 is similar to the optimal equation of Sarup and Wojciechowski [14] for a precipitated cobalt catalyst in a Berty reactor, whereas FT-III3 was found to be the best model by Yates and Satterfield [40] on cobalt measured in a slurry reactor. The kinetic model of Sarup and Wojciechowski [14] was developed with the assumption that the site balance consists of free sites, adsorbed CO and dissociated H_2, while Yates and Satterfield [40] only included CO inhibition.

The WGS reaction rate was optimized with the kinetic expressions in Table 5.7. Due to a high degree of similarity between equations WGS-I5 and WGS-II6, the relative variances are almost equal, 25.0 % and 23.0 %, respectively. The Bartlett's test is unable to discriminate between these models. A parity plot between the experimental and model values of the WGS reaction rates is shown in Figure 5.3. Reaction rate expression WGS-II6 is similar to the optimal model of Lox and Froment [5]. Both models assume that the rate of the WGS reaction is determined by the reaction of adsorbed carbon monoxide and hydroxyl towards a formate intermediate. Our model assumes adsorption of CO and water to be dominant in the site balance, whereas Lox and Froment [5] included inhibition of hydroxyl species only. The corresponding model parameters are also given in Table 5.10.

Both the experimental and the calculated rates of the Fischer-Tropsch and the water gas shift reaction are compared in Figures 5.4- 5.5 at various experimental conditions. The calculated rates stem from models FT-III2 and WGS-II6 with the input

Table 5.10 Final estimates for the parameters of the FT and WGS kinetic models.

Parameter	Dimension	Estimate
WGS-I5 (s_{rel} 21.0 %)		
k_w	mol kg^{-1} s^{-1} MPa^{-2}	1.77 ± 0.04
K_1	MPa^{-1}	2.10 ± 0.04
K_3	MPa^{-1}	24.19 ± 3.14
WGS-II6 (s_{rel} 21.5 %)		
k_w	mol kg^{-1} s^{-1} MPa$^{-1.5}$	1.13 ± 0.01
K_1	MPa^{-1}	2.78 ± 0.04
K_3	MPa^{-1}	12.27 ± 0.94
FT-III2 (s_{rel} 23.7 %)		
k	mol kg^{-1} s^{-1} MPa$^{-1.5}$	0.0488 ± 0.0049
a	MPa^{-1}	0.563 ± 0.094
b	MPa^{-1}	4.05 ± 0.77
FT-III3 (s_{rel} 22.4 %)		
k	mol kg^{-1} s^{-1} MPa^{-2}	0.0556 ± 0.0056
a	MPa^{-1}	0.125 ± 0.069
b	MPa^{-1}	7.00 ± 0.87
FT-IV2 (s_{rel} 22.7 %)		
k	mol kg^{-1} s^{-1} MPa^{-2}	0.0779 ± 0.0157
a	MPa^{-1}	0.536 ± 0.333
b	MPa^{-1}	32.27 ± 8.69

values of the H_2/CO feed ratio and the flow rate, $\Phi^{in}_{v,0}/W$ based on stoichiometry and mass balances of the components present (CO, CO_2, H_2, H_2O). The product composition was determined from gas chromatographic analysis of the gas and from liquid hydrocarbon product samples. The values of n and m were determined from the product composition. In this study, n varied between 2.86-5.04. The ratio of m/n varied between 2.14-2.42. The effluent flow rate was estimated with the average contraction factor calculated at m/n of 2.30. Since the variation of m/n with process conditions is minor, this assumption seems justified.

The effect of the flow rate on the overall rate and rates of the water gas shift and Fischer-Tropsch reaction is demonstrated in Figure 5.4a. As expected, the reaction rates increase with increasing space velocity. There is good agreement between the model calculations and the experimental values. Overall conversion of synthesis gas,

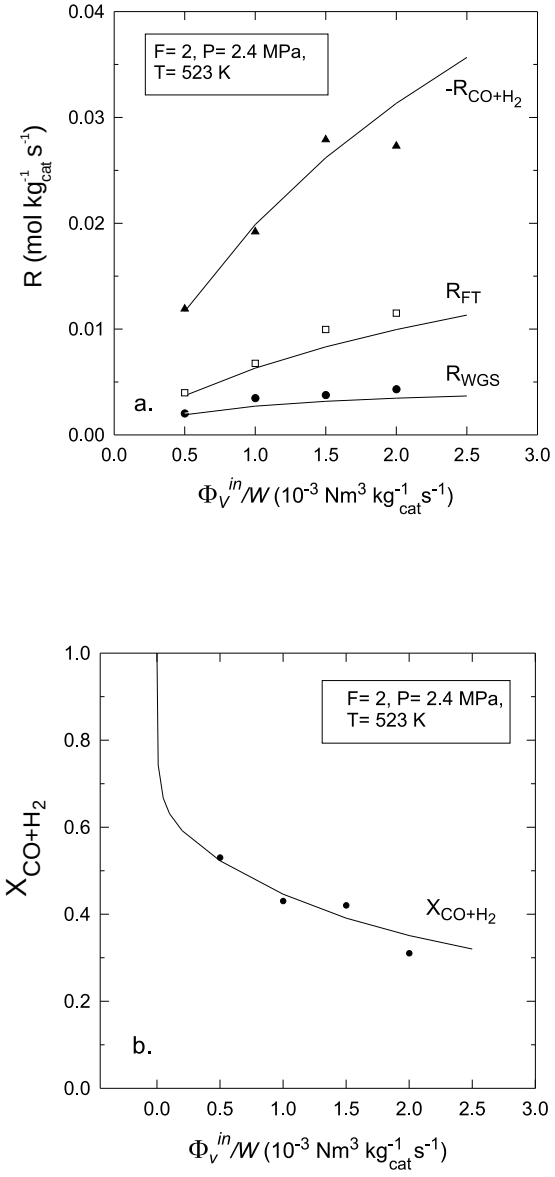

Figure 5.4 Reaction rates for the WGS and FT and total conversion of CO and H_2 (a) and overall conversion of synthesis gas (X_{CO+H_2}) versus space velocity (b). Symbols are experimental values. Lines are model predictions (FT-III2 and WGS-II6).

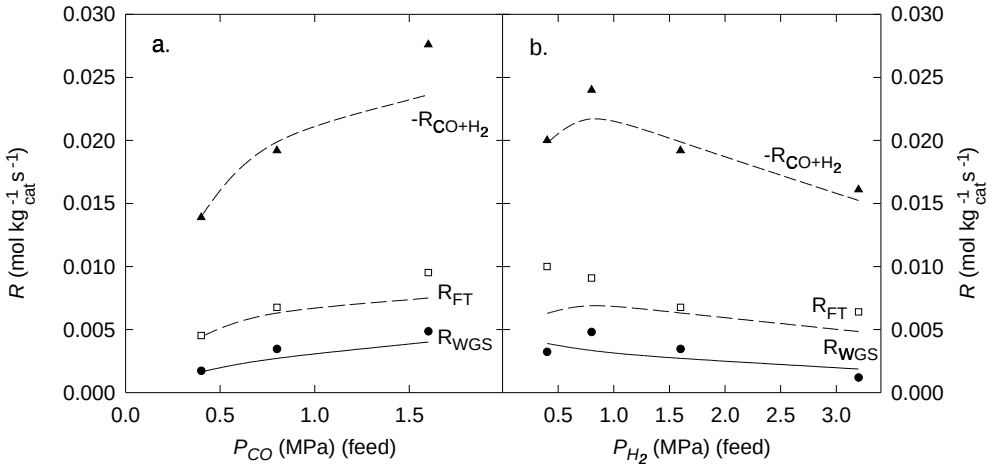

Figure 5.5 Reaction rates for the WGS and FT and total conversion of CO and H_2 versus reactant feed pressures. Symbols are experimental values. Lines are model predictions (FT-III2 and WGS-II6). a: Feed pressure P_{CO}= 0.8 MPa, T= 523 K, Φ_v^{in}/W= 1.0 10^{-3} kg_{cat}^{-1} s^{-1}; b: Feed pressure P_{H_2}= 0.8 MPa, T= 523 K, Φ_v^{in}/W= 1.0 10^{-3} kg_{cat}^{-1} s^{-1}.

X_{CO+H_2}, at the same conditions is accurately predicted with the optimized kinetic expressions and a CSTR reactor model (see Figure 5.4b).

The effect of the individual reactant pressures (P_{CO} and P_{H_2}) in the feed stream is shown in Figures 5.5a-b. The models appear to predict the trends of varying reactant pressures satisfactory. Both the water gas shift as well as the Fischer-Tropsch reaction rate increase with increasing feed pressure of CO (Figure 5.5a). The water pressure decreases with increasing CO pressure causing an increase of the Fischer-Tropsch reaction rate. Figure 5.5b shows that the space time yield and the Fischer-Tropsch reaction rate increase slightly and then decrease monotonically. This is caused by an increase of the hydrogen and water pressure in the reactor with increasing feed pressure of hydrogen. Water is a strong inhibitor on the catalyst and reduces the reaction rates of the hydrocarbon-forming reactions.

5.5 Conclusions

Experiments for the kinetics of the hydrocarbon formation and water gas shift reaction over an iron catalyst were obtained over a wide range of industrially relevant reaction conditions. A number of rate equations were derived on the basis of a detailed set of possible reaction mechanisms. The following conclusions can be made:

1. Two different sites are present on iron catalysts. The iron carbides are active towards hydrocarbon forming reactions, whereas magnetite (Fe_3O_4) seems to be the most active site for the water gas shift reaction.

2. The reaction rate of the Fischer-Tropsch synthesis is determined by the formation of the monomer species (methylene). The best models assume that the rate determining step proceeds via hydrogenation of associative adsorbed CO.

3. Carbon dioxide is formed by the water gas shift reaction. The rate determining step is the formation of a formate intermediate species.

Simulations using the kinetic models derived show good agreement with both experimental data and with some kinetic models from literature.

References

[1] Dry, M.E., The Fischer-Tropsch synthesis, in J.R. Anderson; M. Boudart, eds., *Catalysis-Science and technology*, vol. 1, Springer-Verlag, New York, 1981 pp. 160–255.

[2] Ribeiro, F.H.; Schach von Wittenau, A.E.; Bartholemew, C.H.; Somorjai, G.A., Reproducibility of turnover rates in heterogeneous metal catalysis: compilation of data and guidelines for data analysis, *Catal. Rev.-Sci. Eng.* **1997**, *39*, 49–76.

[3] Bub, G.; Baerns, M., Prediction of the performance of catalytic fixed bed reactors for Fischer-Tropsch synthesis, *Chem. Eng. Sci.* **1980**, *35*, 348–355.

[4] Newsome, D.S., The water-gas shift reaction, *Catal. Rev.-Sci. Eng.* **1980**, *21*, 275–318.

[5] Lox, E.S.; Froment, G.F., Kinetics of the Fischer-Tropsch reaction on a precipitated promoted iron catalyst. 2. Kinetic modeling, *Ind. Eng. Chem. Res.* **1993**, *32*, 71–82.

[6] Wojciechowski, B.W., The kinetics of the Fischer Tropsch synthesis, *Catal. Rev.-Sci. Eng.* **1988**, *30*, 629–702.

[7] Dry, M.E., Advances in Fischer-Tropsch chemistry, *Ind. Eng. Chem. Prod. Res. Dev.* **1976**, *15*, 282–286.

[8] Huff, Jr., G.A.; Satterfield, C.N., Intrinsic kinetics of the Fischer-Tropsch synthesis on a reduced fused-magnetite catalyst, *Ind. Eng. Chem. Process Des. Dev.* **1984**, *23*, 696–705.

[9] Zimmerman, W.H.; Bukur, D.B., Reaction kinetics over iron catalysts used for the Fischer-Tropsch synthesis, *Can. J. Chem. Eng.* **1990**, *68*, 292–301.

[10] Atwood, H.E.; Bennett, C.O., Kinetics of the Fischer-Tropsch reaction over iron, *Ind. Eng. Chem. Process Des. Dev.* **1979**, *18*, 163–170.

[11] Nettelhoff, H.; Kokuun, R.; Ledakowicz, S.; Deckwer, W.-D., Studies on the kinetics of Fischer-Tropsch synthesis in slurry phase, *Ger. Chem. Eng.* **1985**, *8*, 177–185.

[12] Ledakowicz, S.; Nettelhoff, H.; Kokuun, R.; Deckwer, W.-D., Kinetics of the Fischer-Tropsch synthesis in the slurry phase on a potassium-promoted iron catalyst, *Top. Catal.* **1985**, *24*, 1043–1049.

[13] Dixit, R.S.; Tavlarides, L.L., Kinetics of the Fischer-Tropsch synthesis, *Ind. Eng. Chem. Process Des. Dev.* **1983**, *22*, 1–9.

[14] Sarup, B.; Wojciechowski, B.W., Studies of the Fischer-Tropsch synthesis on a cobalt catalyst. II. Kinetics of carbon monoxide conversion to methane and to higher hydrocarbons, *Can. J. Chem. Eng.* **1989**, *67*, 62–74.

[15] Shen, W.J.; Zhou, J.L.; Zhang, B.J., Kinetics of Fischer-Tropsch synthesis over precipitated iron catalyst, *J. Nat. Gas Chem.* **1994**, *4*, 385–400.

[16] Zhang, H.-B.; Schrader, G.L., Characterisation of a fused iron catalyst for Fischer-Tropsch synthesis by in situ laser Raman spectroscopy, *J. Catal.* **1985**, *95*, 325–332.

[17] Lox, E.S.; Marin, G.B.; de Graeve, E.; Bussiere, P., Characterization of a promoted precipitated iron catalyst for Fischer-Tropsch synthesis, *Appl. Catal. A* **1988**, *40*, 197–218.

[18] Shroff, M.D.; Kalakkad, D.S.; Coulter, K.E.; Kòhler, S.D; Harrington, M.S.; Jackson, N.B.; Sault, A.G.; Datye, A.K., Activation of iron precipitated Fischer-Tropsch catalysts, *J. Catal.* **1995**, *156*, 185–207.

[19] Rao, K.R.P.M.; Huggins, F.E.; Mahajan, V.; Huffman, G.P.; Rao, V.U.S.; Bhatt, B.L.; Bukur, D.B.; Davis, B.H.; O'Brien, R.J., Mössbauer spectroscopy study of iron-based catalysts used in Fischer-Tropsch synthesis, *Top. Catal.* **1995**, *2*, 71–78.

[20] Rethwisch, D.G.; Dumesic, J.A., Adsorptive and catalytic properties of supported metal oxides. III. Water-gas shift over supported iron and zinc oxides, *J. Catal.* **1986**, *101*, 35–42.

[21] Ponec, V., Some aspects of the methanation and Fischer-Tropsch synthesis, *Catal. Rev.-Sci. Eng.* **1978**, *18*, 151–171.

[22] Anderson, R.B., *Catalysts for the Fischer-Tropsch synthesis*, vol. 4, Van Nostrand Reinhold, New York **1956**.

[23] Anderson, R.B., *The Fischer-Tropsch synthesis*, Academic Press, New York

1984.

[24] Bell, A.T., Catalytic synthesis of hydrocarbons over group VIII metals. A discussion on the reaction mechanism, *Catal. Rev.-Sci. Eng.* **1981**, *23*, 203–232.

[25] Hindermann, J.P.; Hutchings, G.J.; Kiennemann, A., Mechanistic aspects of the formation of hydrocarbons and alcohols from CO hydrogenation, *Catal. Rev.-Sci. Eng.* **1993**, *35*, 1–127.

[26] Dry, M.E., Conversion of syngas to fuels and chemicals, in *Int. Conf. on Catal. & Catal. Proc.*, Cape Town, South Africa, 1993 pp. 57–66.

[27] Dry, M.E., Practical and theoretical aspects of the catalytic Fischer-Tropsch process, *Appl. Catal. A* **1996**, *138*, 319–344.

[28] Adesina, A.A., Hydrocarbon synthesis via Fischer-Tropsch reaction: travails and triumphs, *Appl. Catal. A* **1996**, *138*, 345–367.

[29] Fischer, F.; Tropsch, H., Uber die Herstellung synthetischer ölgemische (Synthol) durch Aufbau aus Kohlenoxyd und Wasserstoff, *Brennst. Chem.* **1923**, *4*, 276–285.

[30] Schulz, H.; Van Steen, E.; Claeys, M., Olefin formation, hydrogenation and isomerization in the kinetic regime of Fischer-Tropsch synthesis, in *Selective hydrogenation and dehydrogenation*, DGMK, Kassel, Germany, 1993 .

[31] Bianchi, D.; Tau, L.M.; Borcar, S.; Bennett, C.O., Nature of the species on supported iron during CO/H_2 reaction, *J. Catal.* **1983**, *84*, 358–374.

[32] Ponec, V.; Van Barneveld, W.A., The role of chemisorption in Fischer-Tropsch synthesis, *Ind. Eng. Chem. Prod. Res. Des.* **1979**, *4*, 268–271.

[33] Kellner, C.S.; Bell, A.T., The kinetics and mechanism of carbon monoxide hydrogenation over alumina-supported ruthenium, *J. Catal.* **1981**, *70*, 418–432.

[34] Hovi, J.-P.; Lahtinen, J.; Liu, Z.S.; Nieminen, R.M., Monte Carlo study of CO hydrogenation on cobalt model catalysts, *J. Chem. Phys.* **1995**, *102*, 7674–7682.

[35] Graaf, G.H.; Winkelman, J.G.M.; Stamhuis, E.J.; Beenackers, A.A.C.M., Kinetics of the three-phase methanol synthesis, *Chem. Eng. Sci.* **1988**, *43*, 2161–2168.

[36] Froment, G.F.; Hosten, L.H., Catalytic kinetics: modelling, in J.R. Anderson; M. Boudart, eds., *Catalysis. Science and technology*, vol. 2, Springer-Verlag, New York, 1981 pp. 98–170.

[37] Biloen, P.; Sachtler, W.M.H., Mechanism of hydrocarbon synthesis over Fischer-Tropsch catalysts, *Adv. Catal.* **1981**, *30*, 165–216.

[38] Dry, M.E.; Shingles, T.; Boshoff, L.J.; Oosthuizen, G.J., Heats of adsorption on promoted iron surfaces and the role of alkali in Fischer-Tropsch synthesis, *J. Catal.* **1969**, *15*, 190–199.

[39] Yates, I.C.; Satterfield, C.N., Effect of carbon dioxide on the kinetics of the Fischer-Tropsch synthesis on iron catalysts, *Ind. Eng. Chem. Res.* **1989**, *28*, 9–12.

[40] Yates, I.C.; Satterfield, C.N., Intrinsic kinetics of the Fischer-Tropsch synthesis on a cobalt catalyst, *Energy Fuels* **1991**, *5*, 168–173.

[41] Dry, M.E.; Shingles, T.; Boshoff, L.J.; Oosthuizen, G.J., Rate of the Fischer-Tropsch reaction over iron catalysts, *J. Catal.* **1972**, *25*, 99–104.

[42] Whiters, Jr., H.P.; Eleizer, K.F.; Mitchell, J.W., Slurry-phase Fischer-Tropsch synthesis and kinetic studies over supported cobalt carbonyl derived catalysts, *Ind. Eng. Chem. Res.* **1990**, *29*, 1807–1814.

[43] Deckwer, W.-D.; Kokuun, R.; Sanders, E.; Ledakowicz, S., Kinetic studies of Fischer-Tropsch synthesis on suspended Fe/K catalyst. Rate inhibition by CO_2 and H_2O, *Ind. Eng. Chem. Process Des. Dev.* **1986**, *25*, 643–649.

[44] Chanenchuk, C.A.; Yates, I.C.; Satterfield, C.N., The Fischer-Tropsch synthesis with a mechanical mixture of a cobalt catalyst and a copper-based water gas shift catalyst, *Energy Fuels* **1991**, *5*, 847–855.

[45] Van der Laan, G.P.; Beenackers, A.A.C.M., Kinetics and selectivity of the Fischer-Tropsch synthesis. A literature review, Accepted for publication in *Catal. Rev.-Sci. Eng.*

[46] Graaf, G.H.; Sijtsema, P.J.J.M.; Stamhuis, E.J.; Joosten, G.E.H., Chemical equilibria in methanol synthesis, *Chem. Eng. Sci.* **1986**, *41*, 2883–2890.

[47] Bukur, D.B.; Nowicki, L.; Manne, R.K.; Lang, X., Activation studies with a precipitated iron catalyst for Fischer-Tropsch synthesis 2. Reaction studies, *J. Catal.* **1995**, *155*, 366–375.

[48] Westerterp, K.R.; van Swaaij, W.P.M.; Beenackers, A.A.C.M., *Chemical reactor design and operation*, Wiley & Sons, second edn. **1984**.

[49] Jonker, G.H.; Veldsink, J.-W.; Beenackers, A.A.C.M., Intrinsic kinetics of 9-monoenic fatty acid methyl ester hydrogenation over nickel-based catalysts, *Ind. Eng. Chem. Res.* **1997**, *36*, 1567–1579.

[50] Graaf, G.H., *The synthesis of methanol in gas-solid and gas-slurry reactors*, Ph.D. thesis, University of Groningen, The Netherlands **1988**.

[51] Fisher, R.A, *Statistical methods for research workers*, Macmillan, 14th edn. **1970**.